<Original Paper>
Journal of the Korean Society for Nondestructive Testing, Vol. 37, No. 2: 84-90, 2017
ISSN 1225-7842 / eISSN 2287-402X http://dx.doi.org/10.7779/JKSNT.2017.37.2.84

An Efficient Ultrasonic SAFT Imaging for Pulse-Echo Immersion Testing

Hongwei Hu* and Hyunjo Jeong**†

Abstract An ultrasonic synthetic aperture focusing technique (SAFT) using a root mean square (RMS) velocity model is proposed for pulse-echo immersion testing to improve the computational efficiency. Considering the immersion ultrasonic testing of a steel block as an example, three kinds of imaging were studied (B-Scan, SAFT imaging based on ray tracing technology and RMS velocity). The experimental results show that two kinds of SAFT imaging have almost the same imaging performance, while the efficiency of RMS velocity SAFT imaging is almost 25 times greater than the SAFT based on Snell's law.

Keywords: Synthetic Aperture Focusing, Ultrasonic Imaging, Root Mean Square Velocity, Immersion Testing

1. Introduction

Ultrasonic testing is the important means to ensure the key equipment manufacturing quality and service safety of the aerospace, nuclear power, high-speed railway, automobile and so on [1-3]. Immersion ultrasonic testing is widely used in industrial detection because it has the advantages of small non-detection zone, good coupling, easy automation, and high detection capability for defects such as porosities, cracks, interlayers and folds [4,5]. However, in immersion ultrasonic testing, the imaging resolution is easily affected by the factors such as beam propagation characteristics, radiation sidelobes and random noise of the system, which make it difficult to identify and quantify defects [6].

Synthetic Aperture Focusing Technique (SAFT) is an ultrasonic imaging method with high precision, which can be divided into time-domain SAFT imaging and frequency-domain SAFT imaging according to the echo signal processing. SAFT imaging is not affected by the propagation characteristics of Fresnel zone sound field, and the high-resolution images can be obtained by the transducer withsmall aperture and low-frequency, so SAFT imaging is widely used in the field of ultrasonic detection imaging [7,8]. Frequency-domain SAFT imaging is based on phase migration, spectral interpolation, Green's function and so on, and has ahigh computational efficiency [9]. However, for multi-layer media, the frequency-domain SAFT algorithm can only compensate the phase in frequency domain by the phase shift technique, which leads to the over-correction problem and unsatisfactory lateral resolution [10]. In time-domain SAFT imaging, the pulse echo signal is weighted by delay-and-sum (DAS) [11,12]. Due to the differentacoustic impedances in different media, traditional time-domain SAFT imaging uses ray-tracing technique to determine the propagation path of ultrasonic beam and accurately calculate the delay time of ultrasonic beam when propagating in multi-layer media [13]. But this method has the disadvantages of complicated calculation and low imaging efficiency in practical application. Chih-Hsiung Chang et al. [14] proposed that, with the use of focusing probe, the virtual source technology could simplify the delay

[Received: February 11, 2017, Revised: April 5, 2017, Accepted: April 10, 2017] *Changsha University of Science & Technology, 960, 2nd Section, Wanjiali South RD, Changsha, Hunan, P. R. China, **Division of Mechanical and Automotive Engineering, Wonkwang University, Iksan 54231, Korea, † Corresponding Author: hjjeong@wku.ac.kr

overlapping of multi-layer media into a single layer media directly by DAS method. But this method was affected by its detection characteristics, the probe wasfocused at the interface of the media, and the resolution of traditional time-domain SAFT imaging could not be obtained [15].

In order to effectively calculate the propagation time of ultrasonic wave in multi-layer medium and ensure the resolution of SAFT imaging, the root mean square velocity model of seismic wave data processing is introduced to investigate a new SAFT imaging method in this paper [16]. The root mean square velocity model is used to calculate the approximate propagation time of the acoustic beam in multi-layer media, which is compared with the exact propagation time calculated by Snell's law to verify the effectiveness of the model. Taking the immersion ultrasonic imaging of steel block as an example, the imaging efficiency and signal-to-noise ratio (SNR) of B-scan imaging, traditional SAFT imaging, SAFT imaging based on root-mean-square velocity model are compared. The amplitude of the echo signal along the center axis of the defect hole is analyzed, and the echo signal after DAS is enveloped and normalized, the imaging accuracy of the SAFT imaging based on the root mean square velocity model is verified.

2. Root Mean Square Velocity Model of Ultrasonic Propagation in Multi-Layer Media

Fig. 1 shows the ultrasonic propagation in multi-layer media, $c_1 \sim c_L$ are the propagation velocity of ultrasonic wave in the media of layer $1 \sim L$, $m_1 \sim m_{L-1}$ are the thickness of propagation media of layer $1 \sim L$, $\triangle z$ is the vertical propagation distance of ultrasonic wave in the last layer media, and A is the target point in the media of layer L.

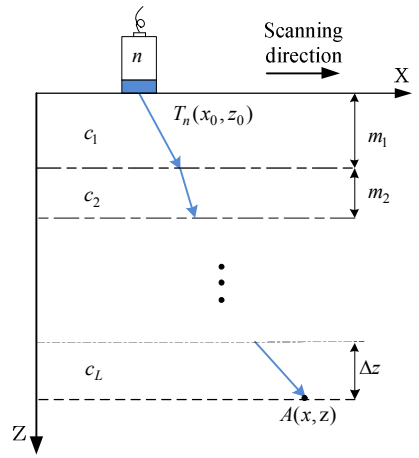

Fig. 1 Multi-layered media ultrasonic propagation

When the ultrasonic beam is perpendicular to the incident, assuming that the ultrasonic propagation velocity is the function $c(z')$ related to the distance z', the propagation time can be obtained after the speed function is integrated, the expression is:

$$t(z) = \int_{z_0}^{z} \frac{1}{c(z')} d(z') \tag{1}$$

where z' is the speed integral variate, the speed integral interval is $z_0 - z$, z_0 is the ordinate value of the probe center position, the target point of the ordinate value.

The acoustic beam propagation time in each layer is obtained by Eq. (1),then the total propagation time is obtained by summation. After the simplification, the propagation time of multi-layer components can be expressed as:

$$t(z) = \left(\sum_{l=1}^{L-1} \frac{m_l}{c_l} \right) + \frac{\Delta z}{c_L} \tag{2}$$

According to Eq. (2), the acoustic beam propagation time $t(z)$ in the multi-layer components is a monotonic function related to the propagation distance $\triangle z$, so the total propagation time is determined by the propagation distance of the sound waves in the

media of layer L. Therefore, the acoustic beam propagation velocity $c(t)$ can be expressed as a function of time t based on the correlation between the propagation velocity, the time and the distance of the acoustic beam, the formula of the root mean square velocity is:

$$c_{\mathrm{rms}} = \sqrt{\frac{1}{t}\int_0^t c(t')^2\,dt'} \tag{3}$$

where t is the total propagation time when the acoustic beam is perpendicularly to the incident in the multi-layer components, t' is the speed integral variate, the speed integral interval is from 0 to t, substituting Eq. (2) into Eq. (3), the root mean square velocity of the acoustic beam propagating in the multi-layer components can be expressed as:

$$c_{\mathrm{rms}}(z) = \sqrt{\frac{\sum_{l=1}^{L-1} c_l m_l + c_L \Delta z}{t(z)}} \tag{4}$$

3. Verification of Root Mean Square Velocity Model

Applying the root - mean - square velocity to the immersion ultrasonic testing, the rootmean square velocity of immersion ultrasonic testing can be expressed as:

$$c_{\mathrm{rms}} = \sqrt{\frac{c_1 m_1 + c_2 m_2}{t_0}} \tag{5}$$

where t_0 is thevertical propagation time of acoustic beam from the center of the probe to the target point:

$$t_0 = \frac{m_1}{c_1} + \frac{m_2}{c_2} \tag{6}$$

According to Eq. (6), the acoustic beam propagation time t_0 is a continuous monotonically increasing function related to the relative propagation distance m_2 under the constant water path. According to Taylor's theorem, when the probe position changes within the effective synthetic aperture, the acoustic beam propagation time can be solved by the Taylor expansion [16,17]:

$$\begin{aligned} t_{\mathrm{rms}}{}^2(x-x_n,z) &= t_0{}^2 + b_2(x-x_n)^2 \\ &+ b_4(x-x_n)^4 + \cdots \end{aligned} \tag{7}$$

where b_2 is the quadratic coefficient of the Taylor expansion:

$$b_2 = \frac{1}{c_{\mathrm{rms}}^2} \tag{8}$$

The acoustic beam propagation time is calculated by Eq. (7), and the higher order part of the Taylor expansion quadratic termis ignored. Substituting Eq. (6) and (8) into Eq. (7), the acoustic beam propagation time based on the root mean square velocity can be obtained:

$$t_{\mathrm{rms}}(x-x_n,z) = \sqrt{t_0{}^2 + \frac{(x-x_n)^2}{c_{\mathrm{rms}}^2}} \tag{9}$$

It can be seen that when the propagation time of acoustic beam in the multi-layer components is obtained by the root mean square velocity, the calculation result is an approximation since the higher order part of the Taylor expansion is neglected. Taking the immersion ultrasonic testing of steel block as an example, assuming the vertical transmission distance of acoustic beam in the steel media is constant, the thickness of the steel block is 35 mm, the water path is 56 mm, the incident angle θ of the sound beam varies in the range of 0°~10°. The accurate propagation time calculated by Snell's law and the approximate propagation time calculated by the root mean square velocity are shown in Fig. 2.

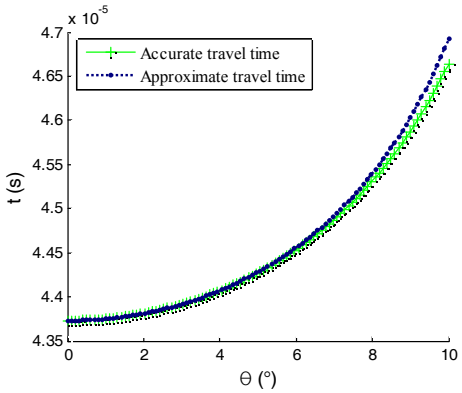

Fig. 2 Water - Steel Crms model validation

4. SAFT Imaging Experiment and Analysis

4.1. Experiments

The standard test block of steel is chosen for immersion ultrasonictesting, as shown in Fig. 3, the target imaging area is 20 mm × 20 mm. The target imaging area is 15 mm away from the top surface of the test block and 22.5 mm away from the left side of the test block, and contains 4 edge through-holes with a diameter of 1.5 mm. A immersion probe with a center frequency of 5 MHz and a aperture of 12.7 mm was used in the experiments, the water path was 56 mm. The CYS-1100 six-axis ultrasonic automatic test bench shown in Fig. 3(b) was used to control the probe to scan from left to right, the scanning step was 0.1 mm. The OLYMPUS-5072P/R pulse transmitter and receiver and PCI9820 data acquisition card were used for data acquisition, the sampling frequency was 60 MHz.

The 200 groups of pulse echo signals were imaged with the horizontal step distance of 0.1 mm, longitudinal discrete step distance of 0.05 mm, and imaging pixel of 200 × 400. The propagation velocity of ultrasonic wave in water is 1480 m/s, the propagation velocity of ultrasonic wave in test block is 5840 m/s. The direct B-scan imaging (B_{scan}) acquired by color modulation is shown in Fig. 4(a), the time-

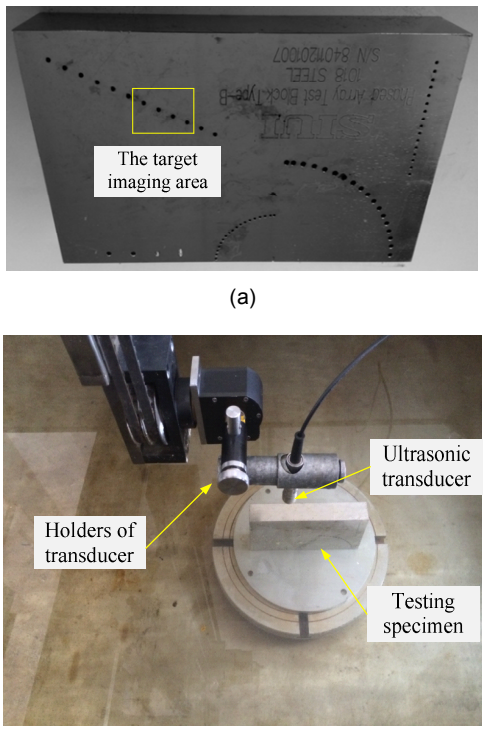

(a)

(b)

Fig. 3 Immersion ultrasonic testing, (a) test specimen; (b) measurement experiment

domain SAFT imaging ($SAFT_{con}$) acquired by the conventional ray-tracing method is shown in Fig. 4(b), and the time-domain SAFT imaging ($SAFT_{rms}$) acquired by the root mean square velocity model is shown in Fig. 4(c). In a PC with Core i3 and a memory of 4G, the SAFT imaging time based on theroot mean square velocity model was 140 s, the SAFT imaging time based on the conventional ray-tracing method was 2052 s, the imaging efficiency was improved about 15 times.

4.2. Analysis of Imaging Resolution

The echo signals of the defective holes along the longitudinal central axis acquired by the different imaging methods shown in Fig. 4 were extracted, and the extracted echo signals were processed by Hilbert transform. Fig. 5

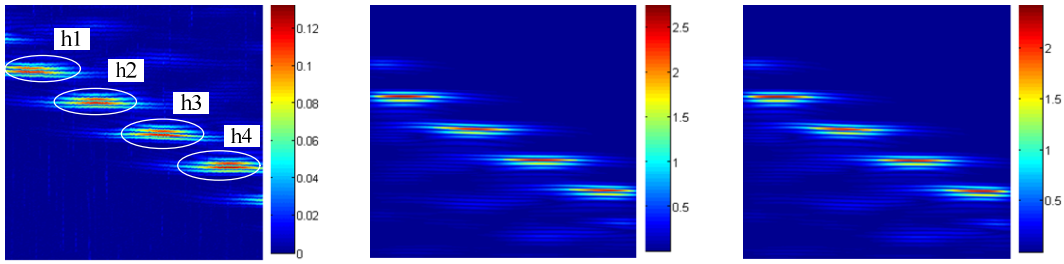

(a) (b) (c)

Fig. 4 The results of three imaging methods; (a) B_{scan}, (b) $SAFT_{con}$, (c) $SAFT_{rms}$

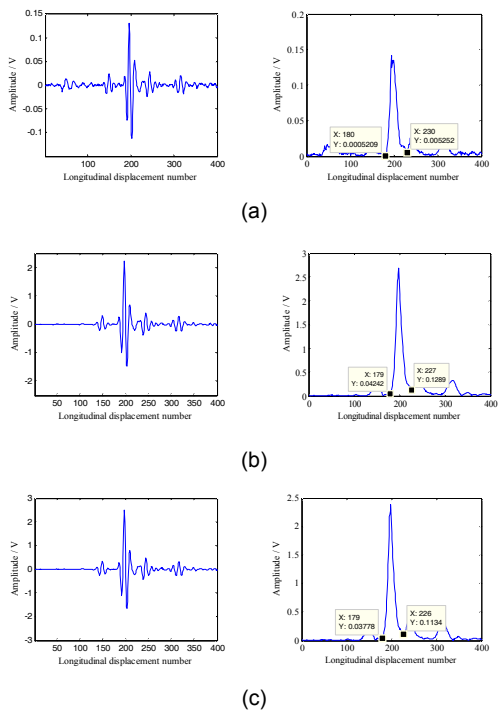

Fig. 5 Longitudinal echo envelope signal of h2 hole with three imaging method; (a) B_{scan}, (b) $SAFT_{con}$, (c) $SAFT_{rms}$

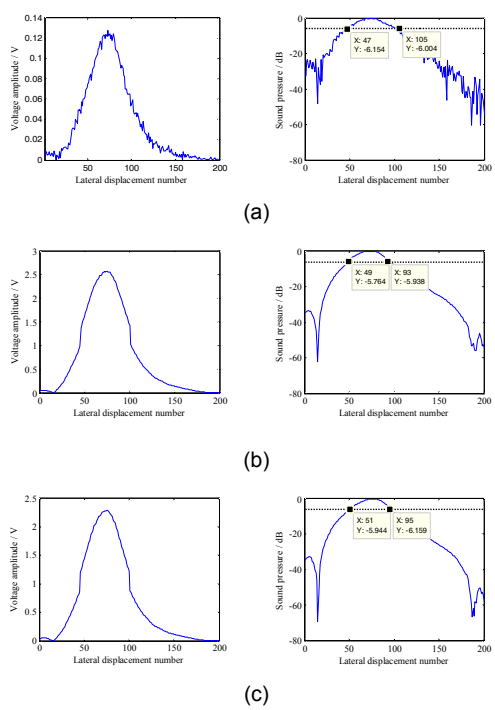

Fig. 6 Lateral voltage amplitude and sound pressure of h2 hole with three imaging methods; (a) B_{scan}, (b) $SAFT_{con}$, (c) $SAFT_{rms}$

shows the echo signals and envelope signals at the center axis of h2 hole under three imaging methods.After analyzing the envelope signals, the longitudinal sizes of the defect holes were 2.5 mm, 2.4 mm, 2.35 mm. It could be seen that the longitudinal resolution of the SAFT imaging based on the root mean square velocity model was consistent with which of the traditional SAFT imaging, and the increase of longitudinal resolution is not obvious with respect to B-scan imaging.

The voltage amplitudes of the defect holes along the lateral central axis acquired by three different imaging methods shown in Fig. 4 were extracted, and the extracted voltage amplitude was normalized. Fig. 6 shows the voltage amplitude and normalized intensity of sound pressure at the transverse central axis of h2 hole under three imaging methods. The lateral dimension of defects was quantified by –6 dB-drop method, and the normalized intensity of sound pressure was analyzed. Then the lateral

Table 1 Defects information about three imaging methods

Imaging characteristics	h1	h2	h3	h4	SNR (dB)
B_{scan} S_g (mm)	2.40	2.50	2.60	2.75	14.10
B_{scan} S_l (mm)	5.50	5.80	6.00	6.30	
$SAFT_{con}$ S_g (mm)	2.25	2.40	2.45	2.50	16.60
$SAFT_{con}$ S_l (mm)	4.30	4.40	4.40	4.60	
$SAFT_{rms}$ S_g (mm)	2.25	2.35	2.45	2.50	16.40
$SAFT_{rms}$ S_l(mm)	4.40	4.40	4.50	4.70	

sizes of defect holes under the three imaging methods were 5.8 mm, 4.4 mm, 4.4 mm. It could be seen that the lateral resolution of the SAFT imaging based on the root mean square velocity model was consistent with which of the traditional SAFT imaging, and it is improved by 24% with respect to B-scan imaging.

The above method was used to analyze the remaining three defect holes, and the longitudinal and lateral sizes (s_g,s_l) of the defect holes under three imaging methods were counted respectively. The maximum voltage amplitude of the speckle noise and the defect hole shown in Fig. 4 were extracted, and the SNR under the three imaging methods were calculated. The statistical results are shown in Table 1, based on the depth of four defect holes, it can be found that the resolution of the SAFT imaging based on the root mean square velocity model is consistent with which of the traditional SAFT imaging. Compared with B-scan imaging, the lateral resolution of traditional SAFT imaging is improved by 22.8%, and the lateral resolution of SAFT imaging based on the root mean square velocity model is increased by 23.3%. As to the imaging SNR, which of the two SAFT imaging methods are basically the sameand 2.3 dB higher than the imaging SNR of B-scan imaging. The results show that the root mean square velocity model can be used to the DAS calculation in SAFT imaging, which provides an efficient SAFT imaging for immersion ultrasonic testing.

5. Conclusions

(1) Taking water-steel media as an example, the accuracy of the delay time calculated by root mean square velocity model was verified by Snell's law. The results show that when the half-power divergence angle is less than 7°, the error of propagation time in water-steel media with the thickness of 56 mm and 35 mm is less than 44 ns.

(2) The imaging resolution and SNR of the SAFT imaging based on the root mean square velocity model is consistent with which of the traditional SAFT imaging. Compared with B-scan imaging, the lateral resolution of the SAFT imaging based on the root mean square velocity model is improved by 23.3%, and the SNR is increased by 2.3 dB. It shows that the SAFT imaging based on the root mean square velocity model is an SAFT imaging for immersion ultrasonic testing with high accuracy.

(3) The imaging efficiency of the SAFT based on the root mean square velocity model is improved almost 15 times than which of the traditional SAFT. It shows that the SAFT imaging based on the root mean square velocity model is an efficient SAFT imaging for immersion ultrasonic testing.

Acknowledgments

This work was supported by the National Natural Science Foundation of China (Grant no. 51205031), and by the National Research Foundation of Korea (Grant no. 2016R1A2B4013953, 2016M2A2A9A03913683).

References

[1] J. Kim, J. Jun and J. Lee, "An application of a magnetic camera for an NDT system

for aging aircraft," *Journal of the Korean society for nondestructive testing*, Vol. 30, No. 3, pp. 212-224 (2010)

[2] C. Li, D. Pain and P. D. Wilcox, B. W. Drinkwater, "Imaging composite material using ultrasonic arrays," *NDT & E International*, Vol. 53, pp. 8-17 (2013)

[3] S. Kolkoori, N. Wrobel and U. Zscherpel and U. Ewert, "A new X-ray backscatter imaging technique for non-destructive testing of aerospace materials," *NDT & E International*, Vol. 70, pp. 41-52 (2015)

[4] E. Sato, M. Shiwa and Y. Shinagawa, T. Ida, S. Yamazoe and A. Sato, "Ultrasonic testing methodfor detection of planar flaws in graphite material," *Materials Transactions*, Vol. 48, No. 6, pp. 1227-1235 (2007)

[5] R. Subbaratnam, S. T. Abraham, B. Venkatraman and B. Raj, "Immersionand TOFD (I-TOFD): a novel combination for examination of lower thicknesses," *Journal of Nondestructive Evaluation*, Vol. 30, No. 3, pp. 137-142 (2011)

[6] T. Olofsson, "Phase shift migration for imaging layered objects and objects immersed in water," *IEEE Transactions on Ultrasonic Ferroelectrics and Frequency Control*, Vol. 57, No. 11, pp. 2522-2530 (2010)

[7] K. Mayer, R. Marklein K. J. Langenberg and T. Kreutter, "Three-dimensional imaging system based on Fourier transform synthetic aperture focusing technique," *Ultrasonics*, Vol. 28, No. 4, pp. 241-255 (1990)

[8] J. A. Jensen, S. I. Nikolov, K. L. Gammelmark, M. H. Pedersen, "Synthetic aperture ultrasound imaging," *Ultrasonics*, Vol. 44, pp. 5-15 (2006)

[9] K. Qin, C. Yang and F. Sun, "Generalized frequency-domain synthetic aperture focusing technique for ultrasonic imaging of irregularly layered objects," *IEEE Transactions on Ultrasonic Ferroelectrics and Frequency Control*, Vol. 61, No. 1, pp. 133-145 (2014)

[10] T. Stepinski, "An implementation of synthetic aperture focusing technique in frequency domain," *IEEE Transactions on Ultrasonic Ferroelectrics and Frequency Control*, Vol. 54, No. 7, pp. 1399-1408 (2007)

[11] J. A. Jensen, S. I. Nikolov, K. L. Gammelmark and M. H. Pedersen, "Synthetic aperture ultrasound imaging," *Ultrasonics*, Vol. 44, pp. 5-15 (2006)

[12] X. Guan, J. He and E. M. Rasselkorde, "A time-domain synthetic aperture ultrasound imaging method for material flaw quantification with validations on small-scale artificial and natural flaws," *Ultrasonics,* Vol. 56, pp. 487-496 (2015)

[13] A. Shlivinski and K. J. Langenberg, "Defect imaging with elastic waves in inhomogeneous-anisotropic materials with composite geometries," *Ultrasonics*, Vol. 49(1), pp. 89-104 (2007)

[14] C. H. Chang, Y. F. Chang and Y. Ma and K. K. Shung, "Reliable estimation of virtual source position for SAFT imaging," *IEEE Transactions on Ultrasonic Ferroelectrics and Frequency Control*, Vol. 60, No. 2, pp. 356-363 (2013)

[15] T. Scharrer, M. Schrapp, S. J. Rupitsch, A. Sutor and R. Lerch, "Ultrasonic imaging of complex specimens by processing multiple incident angles in full-angle synthetic aperture focusing technique," *IEEE Transactions on Ultrasonic Ferroelectrics and Frequency Control*, Vol. 61, No. 5, pp. 830-839 (2014)

[16] M. Taner and F. Koehler, "Velocity spectra-digital computer derivation applications of velocity functions," *Geophysics*, Vol. 34, No. 6, pp. 859-881 (1969)

[17] A. H. Kleyn, "Seismic Reflection Interpretation," Elsevier Applied Science Publishers, New York, pp. 73-76 (1983)